Dietary resveratrol intervention improves lipid homeostasis via attenuating HFD-induced fecal chenodeoxycholic acid and jejunum SR-B1 elevation

Juan Pang
Sun Yat-sen University
Fitore Raka
University of Toronto
Alya Abbas Heirali
University of Toronto
Weijuan Shao
University of Toronto
Dinghui Liu
Sun Yat-sen University
Jianqiu Gu
The First Hospital of China Medical University
Jia Nuo Feng
University of Toronto
Chieko Mineo
The University of Texas Southwestern Medical Center
Philip Shaul
The University of Texas Southwestern Medical Center https://orcid.org/0000-0003-1157-4002
Xiaoxian Qian
Sun Yat-sen University
Bryan Coburn
University of Toronto https://orcid.org/0000-0003-0150-4510
Khosrow Adeli
Toronto
Wenhua Ling
Sun Yat-sen University
Tianru Jin (tianru.jin@utoronto.ca)
University Health Network and University of Toronto https://orcid.org/0000-0002-0307-7391

Article

Keywords: Bile acids, Chylomicron secretion, Dietary resveratrol intervention, Fecal Microbiome Transplantation, Metabolomics analysis, Scavenger receptor class B type 1 (SR-B1)

Posted Date: September 27th, 2022

DOI: https://doi.org/10.21203/rs.3.rs-2050101/v1

Version of Record: A version of this preprint was published at Nature Communications on May 9th, 2023. See the published version at https://doi.org/10.1038/s41467-023-38259-1.

Abstract

Two common features of dietary polyphenols have hampered our mechanistic understanding of their metabolic beneficial effects for decades: targeting multiple organs and extremely low bioavailability. We show here that resveratrol intervention (REV-I) in high fat diet (HFD)-challenged mice inhibited chylomicron secretion, associated with reduced jejunal but not hepatic SR-B1 expression. Intestinal-mucosa-specific SR-B1-/- mice on HFD challenge exhibited improved lipid homeostasis but showed virtually no further response to REV-I. The SR-B1 inhibitor BLT-1 and REV-I generated no additive effect on improving lipid homeostasis. SR-B1 expression in the Caco-2 cell line cannot be repressed by pure resveratrol while fecal-microbiota transplantation from mice on REV-I suppressed jejunal SR-B1 in recipient mice. REV-I reduced fecal levels of bile acids including chenodeoxycholic acid (CDCA), while CDCA stimulated FXR, NF-κB and SR-B1 in Caco-2 cells. We conclude that gut microbiome is the primary target of REV-I, and REV-I improves lipid homeostasis at least partially via attenuating CDCA-stimulated gut SR-B1 elevation.

Introduction

Many natural products, available commercially in concentrated formulations, have been shown to possess metabolic beneficial effects and are promoted worldwide for the prevention or even the treatment of metabolic disorders including type 2 diabetes (T2D), nonalcoholic fatty liver disease (NAFLD), and cardiovascular diseases (CVD). Among them, dietary polyphenols of plant origin including resveratrol, have attracted the most attention of biomedical researchers, drug developers and nutritional scientists. These compounds were shown to improve insulin signaling and energy homeostasis in animal models and human subjects[1–5]. For decades, two fundamental challenges have limited our mechanistic understanding of their functions. Firstly, those polyphenols were often shown to target multiple organs and signaling cascades, without a defined receptor. Secondly, the bioavailability of those polyphenols is always extremely low. After consumption of a large amount of a phenolic compound, its maximum plasma concentration rarely exceeds 1 μM. Thus, dietary polyphenols may exert their functions initially in the gut where their concentrations are the highest, possibly by targeting gut microbiota. They may change gut microbiota profiles, regulate the production of bacterial products or fermentation products of the food, or exert their functions via various gut metabolites[6–9]. Indeed, several recent studies suggested that beneficial effects of resveratrol intervention (REV-I) are associated with alterations in the gut microbiome[4,10,11].

Intestinal production of ApoB48-containing chylomicrons is significantly increased during insulin resistance, while its clearance is impaired in T2D or NAFLD[12,13]. Chylomicrons are major forms of circulating TG-rich lipoprotein (TRL), while another one is very low-density lipoprotein (VLDL), which is produced in the liver. The major lipid composition of chylomicrons is triglyceride (TG), followed by dietary cholesterol in the form of cholesteryl ester. Studies have shown that postprandial hypertriglyceridemia is a powerful predictor of CVD, stronger than fasting hypertriglyceridemia[14]. Chylomicron remnants after

lipolysis can enter the arterial intima, and remnant cholesterol can accumulate in intimal foam cells to form atherosclerotic plaques[15,16]. Chylomicron remnants can also be taken up by the liver, raising the risk of NAFLD[17,18].

Chylomicron production involves dietary fatty acid (FA) uptake, TG synthesis, chylomicron assembly and secretion from apical to basolateral enterocytes[19,20]. Multiple lipid transporters participate in the process, including cluster determinant 36 (CD36)[21], scavenger receptor class B type 1 (SR-B1)[22], and FA transport protein 4 (FATP4)[23]. Among them, SR-B1 was shown to be elevated the most in the small intestine of insulin-resistant hamster model, associated with increased postprandial TG and TRL accumulation[22]. Furthermore, SR-B1 knockout (KO) mice or mice treated with SR-B1 inhibitor displayed less chylomicron production[22,24].

In the current study, we revealed a novel function of REV-I: inhibition of gut chylomicron secretion. Gut but not liver SR-B1 was found to be downregulated by REV-I. Importantly, the *in vivo* repression of REV-I on SR-B1 and chylomicron secretion could not be observed by direct resveratrol treatment in the Caco-2 cell line. We then observed that Caco-2 cells treated with fecal extract (FE) from mice on HFD plus REV-I showed relatively lower levels of SR-B1, when compared with Caco-2 cells treated with FE from HFD mice in the absence of REV-I. Fecal microbiota transplantation (FMT) revealed the effect of feces from mice that received REV-I on improving fat tolerance and reducing jejunal SR-B1. Finally, we conducted gut microbiome analyses and metabolomics analyses of FE, leading to the recognition that the primary bile acid chenodeoxycholic acid (CDCA) can stimulate NF-κB and SR-B1 while REV-I attenuates HFD challenge-induced fecal CDCA elevation.

Results

REV-I reduces chylomicron production in HFD-challenged mice- As shown (Fig. 1A), 6-week-old male mice were fed with LFD, HFD, or HFD + REV-I (HFR) for 8 weeks. REV-I reduced HFD-induced body weight gain (Fig. 1B-C), decreased fat mass and hepatic fat content (Figure S1A-C). There was no difference in food intake among 3 groups of mice (Figure S1D). REV-I improved glucose and insulin tolerance, accompanied with reduced fasting glucose and insulin levels (Fig. 1D-G). When adjusted for basal blood glucose level, the improvement in insulin tolerance was virtually absent in the current experimental setting (Figure S1E). Furthermore, REV-I reduced the level of fasting TG but not non-esterified FA (NEFA) (Fig. 1H-I).

Plasma TG level is determined by the balance of chylomicron production, hepatic VLDL production, and TRL clearance. When lipoprotein lipase (LPL) activity was blocked with poloxamer 407 in overnight fasted mice, there was no difference in plasma TG level (Figure S1F), indicating that REV-I in the current experimental setting did not significantly affect hepatic VLDL production during fasting. Consistently, REV-I did not attenuate HFD-induced fasting ApoB48 and TG content in TG-rich lipoprotein (TRL) (Figure S1G-H). Moreover, plasma LPL activity was similar among the three groups of mice (Figure S1I). In postprandial conditions, plasma TG accumulation in mice challenged with olive oil was reduced with REV-I (Fig. 1J). In isolated TRL (mainly chylomicrons), TG content and ApoB48 level were reduced in mice

with REV-I (Fig. 1K-L). These observations suggest that REV-I reduces plasma TG by inhibiting chylomicron production in the fed state. Figure 1M summarizes metabolic effects of REV-I observed in this set of mice.

REV-I reduces jejunal but not liver SR-B1- Dietary lipid intake and *de novo* lipogenesis result in gut lipid droplet accumulation, which are then packaged as chylomicrons, or go through FA β-oxidation. Chylomicrons are secreted through the basolateral membrane into the lacteals, where they join lymph to become chyle (Fig. 2A). In a separate set of mice with or without 8-week REV-I, we measured TG intake and its fecal output. HFD challenge led to elevated TG intake and fecal TG output, but REV-I did not reduce TG intake or increase its output (Fig. 2B-C), suggesting that REV-I did not affect intestinal TG absorption. TG accumulation in the intestine remained at comparable levels (Fig. 2D). We then measured jejunal expression of genes that are associated with lipid metabolism. REV-I did not affect expression of genes that are related to TG uptake, *de novo* lipogenesis, or chylomicron assembly, but significantly attenuated the stimulation of HFD on expression of *Scarb1* (which encodes SR-B1) and increased expression of genes that are responsible for lipolysis and FA β-oxidation (Fig. 2E and Table S4). Importantly, jejunal but not liver SR-B1 level was reduced by 54% by REV-I (Fig. 2F). SR-B1 at gut apical membrane is known to mediate lipid sensing and chylomicron secretion[25]. We show here that REV-I also attenuated apical migration of SR-B1 (Fig. 2G-H).

Intestinal mucosa specific SR-B1 KO mice show lack of further response to REV-I- To further explore the involvement of gut SR-B1 on mediating functions of REV-I, experiments were then conducted in intestinal mucosa-specific SR-B1 KO (*iScarb1*$^{-/-}$) mice (Fig. 3A). *iScarb1*$^{-/-}$ and the control *Scarb1*$^{fl/fl}$ mice were fed with HFD, with or without REV-I for 8 weeks. Figure S2A-D shows our validation on intestinal mucosa-specific KO of SR-B1 and our observation that at the age of 6 weeks, basal body weight and fasting TG level were comparable in *iScarb1*$^{-/-}$ and *control* mice. Following HFD challenge, *iScarb1*$^{-/-}$ mice showed lower body weight gain (Fig. 3B-C). Concomitant REV-I for 8 weeks reduced body weight gain in control but not *iScarb1*$^{-/-}$ mice (Fig. 3C). In control but not *iScarb1*$^{-/-}$ mice, REV-I reduced fat mass, while liver weight to body weight ratio of the four groups of mice were comparable (Figure S2E-F). Figure 3D-F show that improvement on glucose and insulin tolerance by REV-I in control mice were absent in *iScarb1*$^{-/-}$ mice. Importantly, *iScarb1*$^{-/-}$ mice showed lower fasting and postprandial plasma TG accumulation (Fig. 3G-H). Chylomicron production, determined by assessing TG and ApoB48 levels in TRL, was also decreased in *iScarb1*$^{-/-}$ mice (Fig. 3I-J). However, REV-I generated no further reduction in *iScarb1*$^{-/-}$ mice (Fig. 3I-J). Moreover, REV-I enhanced expression of the lipolysis genes *Cpt1a* and *Acadm* in *Scarb1*$^{fl/fl}$ mice but not in *iScarb1*$^{-/-}$ mice (Fig. 3K). Figure 3L summarizes results of REV-I in the above four groups of mice, suggesting that gut SR-B1 is a major target of REV-I in improving energy homeostasis and reducing chylomicron secretion.

BLT-1 gavage generates no additive effect with REV-I- We then further tested the role of gut SR-B1 in mediating effects of REV-I by orally applying BLT-1, a specific SR-B1 inhibitor. C57BL/6J mice were fed with LFD, HFD, or HFD with REV-I (HFR) for 4 weeks. The HFD and HFR groups were then further divided

into two subgroups, with or without daily gavage of BLT-1 for two more weeks (Fig. 4A). BLT-1 or REV-I attenuated HFD-induced body weight gain; but they generated no additive effect (Fig. 4B-C). Two-week BLT-1 gavage, or 6-week REV-I, or combined use of them, generated no attenuation on epididymal fat mass increase induced by HFD, and did not change liver weight to body weight ratio (Fig. 4D-E). Furthermore, BLT-1 did not reduce fasting glucose level, while REV-I did (Fig. 4F). Mice in all three treatment groups showed decreased fasting and postprandial TG levels and reduced chylomicron production (Fig. 4G-J). Similarly, the combined use of REV-I and BLT-1 had no additive effect (Fig. 4G-J). Thus, REV-I generated no further beneficial effects on lipid homeostasis when function of gut SR-B1 was chemically inhibited by BLT-1.

REV-I represses jejunal SR-B1 involving reduced transcriptional activity of NF-κB-p65- To explore how can REV-I downregulate SR-B1, we located transcriptional factor binding motifs on *Scarb1* promoter, including that of SREBP-1. Western blotting, however, showed comparable jejunal SREBP-1 levels in LFD, HFD, and HFR groups (Fig. 5A). Although qRT-PCR showed elevated jejunal *Srebf1* (which encodes SREBP-1) in HFD mice, REV-I did not repress it and generated no effect on expression of the three SREBP-1 downstream targets (Fig. 5B). Within human and rodent *SCARB1* or *Scarb1* promoters, we located a conserved binding motif for NF-κB-p65 (Fig. 5C). Eight-week HFD challenge increased jejunal NF-κB-p65 expression, while REV-I blocked the increase (Fig. 5D). Such blockage was associated with the inhibition of genes that are members of the NF-κB signaling pathway (Fig. 5E and Table S5). Expressions of key members of NLRP3 inflammasome were also repressed by REV-I (Fig. 5F). Using ChIP and qChIP, we observed increased interactions between NF-κB-p65 or RNA Polymerase II with the *Scarb1* promoter in mice on HFD, while REV-I attenuated their interactions (Fig. 5G-J).

The resveratrol compound does not repress SR-B1 in Caco-2 cells- In Caco-2 cells treated with resveratrol at dosages that did not reduce cell viability (1, 5, and 25 μM), we observed no repression on SR-B1 or NF-κB-p65 or genes that encode them (Figure S3A-C). We then established the intestinal barrier model by culturing Caco-2 cells in microporous PET transwell inserts for 21 days, allowing Caco-2 cells to be differentiated into monolayers with polarity (Figure S3D). Lipid micelle was shown to stimulate chylomicron secretion, detected by measuring BODIPY labelled C_{12} FA secreted into the lower compartment. Resveratrol treatment, however, did not reduce it (Figure S3E). Thus, *in vivo* down-regulation of NF-κB, SR-B1, and chylomicron secretion by REV-I, could not be reproduced in our *in vitro* experimental settings.

The inhibitory effect of REV-I on SR-B1 involves gut microbiota- The discrepancy between *in vivo* and *in vitro* effects of resveratrol on SR-B1 suggests that jejunal SR-B1 regulation involves entities that are absent *in vitro*, such as gut microbiota. We hence collected fresh feces from mice on HFD or HFR for 8 weeks. Following sonication and filtration, we collected sterile FE. When HFD-FE or HFR-FE was diluted 150-fold or higher, we did not see their repression on Caco-2 cell viability (Figure S4A-B). When these FEs (diluted at 1:1200) were applied to Caco-2-derived intestinal barrier model, HFR-FE treated cells showed relatively lower levels of chylomicron secretion (Figure S4C). Furthermore, the stimulatory effect of HFD-FE on Caco-2 SR-B1 and NF-kB p65 expression was absent when HFR-FE was applied (Figure S4D-E). We

then treated sterile FEs at 95℃ for 5 min before they were applied to Caco-2 cells. As shown (Figure S4F), heated HFR-FE treated Caco-2 showed relatively lower levels of SR-B1 when compared with Caco-2 treated with heated HFD-FE. We hence suggest that *in vivo* repression of gut NF-κB/SR-B1 signaling by REV-I is likely involving certain heat-stable products present in feces. If they stimulate NF-κB/SR-B1, REV-I will reduce their production, and vise versa.

Sung *et al* have reported that oral resveratrol administration generated taxonomic and functional changes in the gut microbiome of diet-induced obese mice. They also demonstrated that FMT from resveratrol-fed donor mice was sufficient to improve glucose disposal in the obese recipient mice[4]. Here we conducted a 12-day FMT, with either fecal slurry from HFD-fed mice (HFD-FMT) or HFR-fed mice (HFR-FMT). C57BL/6J mice fed with LFD or HFD for 4 weeks were treated with designated FMT on day 1, 3 and 5 following overnight fasting and PEG3350 treatment to eliminate recipient gut microbiota (Fig. 6A). We also included the 3rd sub-group for both LFD and HFD-fed mice, designated as HFD-FMT + R, in which mice received fecal slurry from HFD-fed mice also received resveratrol gavage (500 mg/kg body weight) on day 1, 3 and 5. OGTT and fat tolerance test (FTT) were conducted on day 7 and day 12, respectively (Fig. 6A).

We designed this short-term FMT, aimed to ask whether repression on gut SR-B1 can occur ahead of the known function of FMT on lowering body weight or glucose homeostasis[4]. As shown, on day 7, we did not see affected glucose tolerance within either LFD or HFD group (Fig. 6B) and FMT did not affect body weight gain among mice in LFD or HFD group (Fig. 6C-D). We also did not see an effect of given FMT on fasting TG levels yet (Fig. 6E). When FTT was conducted on day 12, in which mice were challenged with olive oil after the blockage of plasma LPL activity. In the LFD group, mice received HFD-FMT + R showed the highest level of postprandial TG (Fig. 6F). Although we cannot provide a clear explanation for such elevation, this observation supports our view that lipid homeostatic effect of resveratrol cannot be achieved in a short term on its own (3 times gavage on day 1, 3 and 5 for current study), because longer time is required for resveratrol to “re-shape” gut microbiome. Importantly, in the HFD group, mice that received HFR-FMT showed lower postprandial TG level when compared with mice received HFD-FMT (Fig. 6F). In isolated postprandial TRL, HFD mice received HFR-FMT had lower TG content and ApoB48 level when compared with that received HFD-FMT, although the difference did not reach statistical significance (Fig. 6G-H). Finally, jejunal SR-B1 level in HFD mice received HFR-FMT was lower than that received HFD-FMT (Fig. 6I).

REV-I changes gut microbiome composition and attenuates HFD-induced fecal CDCA elevation- We then investigated the effect of REV-I on gut microbiome composition in mice on HFD challenge. When three-dimensional principal coordinate analysis (PCoA) was used to visualize Bray-Curtis beta-diversity, the fecal samples (from HFD and HFR treated mice) were not statistically separated based on groups (P = 0.133 by PERMANOVA test, Figure S5A). Gut microbiota compositions at phylum and genus levels were then analyzed. At the phylum level, there was a decreasing tendency in the relative abundance of *Firmicutes* while the relative abundance of *Bacteroidetes* as well as the ratio of *Bacteroidetes*/ *Firmicutes* were increased in the HFR group (Figure S5B-C). At the genus level, *Eubacterium*_brachy_group,

Erythrobacter and *Streptomyces* were decreased while *Eubacterium*_nodatum_group and *Bacteroides* were increased in the HFR group (Figure S5D). We have also profiled gut microbiome with mouse caecum contents in a separated set of mice, including mice treated with LFD, HFD or HFD + REV-I for 8 weeks. When principal coordinate analysis (PCoA) was used to visualize Bray-Curtis beta diversity, we found that caecum content samples were separated based on diet (Figure S5E). Shannon Diversity index, inverse Simpson and richness (observed taxa) metrics were utilized to analyze alpha-diversity differences. Caecum samples from HFD-fed mice showed much lower alpha-diversity when compared to LFD or HFR-fed mice (Figure S5F). Figure S5G shows the taxonomic summary of phyla in the three groups of mice. In contrast to fecal sample gut microbiome profiling, we did not see elevated *Bacteroidetes*/ *Firmicutes* ratio with REV-I. Together, although the above results showed that REV-I changed gut microbiota composition, this general profiling did not lead to a direct clue on further identifying entities in FEs that may directly regulate gut SR-B1 expression.

We hence asked whether certain metabolites of resveratrol repress SR-B1. *Trans*-resveratrol can be degraded into three major metabolites by gut microbiota, including dihydroresveratrol (DHR), lunularin and 3,4'-dihydroxy-*trans*-stilbene. The third one is not commercially available (Figure S6A). When Caco-2 cells were treated with 25 μM DHR or lunularin for 8 h, there was no appreciable effect on *SCARB1* or *RELA* expression (Figure S6B-C). In Caco-2 cells pre-treated with LPS and IFNγ, DHR exerted appreciable anti-inflammatory effect, as it inhibited expression of *IL6* and *TNF* (which encodes human IL-6 and TNF-α, respectively). The treatment, however, did not reduce expression of *SCARB1* and *RELA* (Figure S6D). Thus, although DHR does possess direct anti-inflammatory effect, it is not the compound in feces that is directly involved in regulating SR-B1 expression.

Since we cannot obtain a direct clue from gut microbiome analyses on identifying entities that may directly regulate gut SR-B1 by HFD and REV-I, we did metabolomics profiling of FEs from HFD and HFR mice. HFR-FE was also heated at 95°C for 5 min, referring to HRH-FE. Through LC-MS/MS analysis, we detected 2053 metabolites. Principal component analysis (PCA) revealed that composition of metabolites in HFD-FE and HFR-FE are different, and after heat treatment, a large portion of metabolites in HFR-FE was transformed (Fig. 7A). We then conducted differential analysis and identified 238 differential metabolites between HFR and HFD groups, and 432 differential metabolites between HRH and HFD groups. Top 10 increased and decreased metabolites in the HFR group, compared with the HFD group, are shown in Figure S7A. Biological activities of those metabolites remained largely unknown. We picked 4'-hydroxyflavone for a further test in Caco-2 cells as this metabolite was reported to inhibit SREBP-1[26]. As shown, although 4'-hydroxyflavone repressed expression of genes that encode human IL-6, IL-1β and MCP-1, it did not directly repress the expression of *SCARB1* or *RELA* (Figure S7B).

We then conducted the KEGG pathway enrichment analysis and the results suggested that sphingolipid metabolism and bile acid metabolism-related pathways were mostly modulated by REV-I (Fig. 7B). As FE from HFR-fed mice before or after heating showed a comparable effect on SR-B1 expression, we looked for compounds with comparable levels in HFR-FE and HRH-FE. K-Means clustering analysis was performed in which differential compounds were divided into 7 subclasses according to their relative

abundance in different groups. Only subclass 3 and 7 showed comparable levels in HFR-FE and HRH-FE (Fig. 7C). Subclass 3 mainly contains sphingolipids, bile acids and certain amino acids, while subclass 7 consists of organic acid derivatives, benzene derivatives and certain other amino acids. Through differential analysis, chenodeoxycholic acid (CDCA) and deoxycholic acid (DCA) were shown to be reduced in HFR-FE when compared with that in HFD-FE (Figure S7C). This is also true when HRH-FE was compared with HFD-FE (Figure S7D). We also conducted a joint analysis of microbiome and metabolomics data. Interestingly, there was a positive correlation between the abundance of *Eubacterium*_brachy_group, a differential genus, and fecal CDCA or DCA levels (Figure S7E-F).

CDCA or a synthetic FXR agonist stimulates SR-B1 in Caco-2 cells- CDCA and DCA are natural Farnesoid X Receptor (FXR) agonists while CDCA is the most potent one. We asked whether CDCA/FXR signaling activation regulates SR-B1 in Caco-2 cells. Both CDCA and GW4064, a synthetic FXR agonist, were shown to activate *NR1H4* (which encodes human FXR) and its downstream target *NR0B2* (which encodes human small heterodimer partner, SHP) in Caco-2 cells. Importantly, consistent with our anticipation, CDCA and GW4064 directly activated *SCARB1*, *RELA* and *IL6* in Caco-2 cells (Fig. 7D). We then assessed jejunal expression of FXR signaling in mice on LFD, HFD, or HFR for 8 weeks. Although HFD feeding did not significantly increase expression of jejunal *Nr1h4*, REV-I significantly repressed its expression. HFD feeding increased jejunal levels of *Nr0b2* and *Fgf15*, while elevated *Fgf15* expression was significantly attenuated by REV-I. For other two target genes of FXR, no appreciable difference was noted in the three groups of mice (Fig. 7E). We suggest that fecal bile acid homeostasis and its associated gut FXR signaling activity are likely among the downstream targets of resveratrol-gut microbiota interaction on repressing gut SR-B1.

Discussion

Although numerous studies have shown profound effects of dietary polyphenol interventions on improving insulin signaling and attenuating dyslipidemia; for decades, mechanisms underlying these beneficial effects remain to be elusive. More and more attention has been made to contributions of gut microbiome toward metabolic homeostasis[2,4,9,11,27]. Bringing gut microbiome and its associate gut fecal metabolites into mechanistic understating of dietary polyphenol intervention will help us to resolve the puzzle of why those interventions target multiple organs with extremely low plasma bioavailability. We show here that inhibition of chylomicron secretion is among key functions of REV-I, and the inhibition involves SR-B1 repression specifically in the gut. Moreover, we observed the beneficial effect of REV-I on attenuating HFD-induced fecal CDCA and DCA elevation, while CDCA, a potent natural FXR agonist, stimulated FXR and SR-B1 in Caco-2 cells. We hence suggest that REV-I targets gut microbiome, leading to the regulation of gut bile acid homeostasis and the attenuation of SR-B1-mediated gut chylomicron secretion.

The high concentration of resveratrol in red wine provides an explanation for the “French paradox,” referring to the fact that French people have lower rates of CVD although they consume more saturated fat-rich diets. In an early clinical trial, Dash *et al* assessed effect of resveratrol in overweight and obese

human subjects. They reported that high-dose (1–2 grams daily) resveratrol reduced both intestinal and hepatic lipoprotein particle production[28]. ApoB-48 production rate in those subjects receiving 2-week resveratrol treatment was reduced by 22%[28]. In this clinical investigation, however, potential involvement of gut SR-B1 inhibition was not assessed.

Approximately 50,000 PubMed publications have been generated to date on resveratrol, curcumin, and anthocyanin, the three major dietary polyphenols. A common feature of those plant-derived "nutraceuticals" is the lack of defined receptors. Resveratrol and curcumin were also defined as "pan-assay interference compounds", not suitable for high-throughput screening tools in the drug development industry. Those dietary polyphenols were shown to target multiple organs and regulate multiple signaling cascades. This feature is shared by known drugs including digoxin, acetylsalicylic acid, artemisinin, and metformin[29]. Such feature also makes the journey for the mechanistic understanding of their biological functions relatively lengthy.

SR-B1 is a multifunctional scavenger receptor widely expressed in metabolic active tissues such as liver, adrenal gland, intestine and vascular endothelium[30–32]. In the liver, it serves as the HDL receptor and mediates reverse cholesterol transport to prevent atherosclerosis[33]. In vascular endothelial cells, it drives LDL transcytosis to promote atherosclerosis[34]. In mouse small intestine, we reported that expression of SR-B1 was the highest in the jejunum among the intestinal segments, and jejunal SR-B1 over-expression was associated with chylomicron over-production[22]. We suggest that it is necessary to bring tissue-specific transgenic mouse models into our investigations for dissecting their functions in each cell lineage. In the current study, we showed that 8-week REV-I prevented HFD-induced jejunal SR-B1 over-expression and reduced chylomicron secretion. Utilizing intestinal mucosa-specific SR-B1 KO mouse model and the chemical inhibitor BLT-1, we verified that targeting jejunal SR-B1 is a key mechanism for REV-I in attenuating chylomicron secretion.

More and more attention has been made on the role of gut microbiome in regulating metabolic homeostasis[3,6,9,10], including its role in mediating the beneficial effects of REV-I[4,10,11]. Mechanistic insights on its involvement, however, need to be further explored. There are several ways that interactions among dietary polyphenols, gut microbiome, and ingested food, can influence metabolic homeostasis. Firstly, gut microbiota metabolites of a polyphenol may exert certain function. In studying anthocyanin, we observed that its microbial metabolite protocatechuic acid (PCA) possesses remarkable anti-atherogenic effect[8]. Secondly, dietary polyphenols may reverse gut microbial dysbiosis caused by HFD[10]. Gut microbiota may also produce certain products with metabolic functions. Administration of *Akkermensia muciniphila* (*A. muciniphila*) or its out-membrane protein Amun_1100 was shown to improve metabolic homeostasis or the gut barrier[35]. Furthermore, the drastic expansion of *A. muciniphila* was observed in HFD-fed mice with dietary intervention utilizing polyphenol-rich extract from cranberry[36]. Finally, dietary polyphenol intervention will affect fermentation processes of gut microbiota on ingested food. It is well known that short-chain FAs (SCFAs), derived from intestinal fermentation, exert multiple functions in the gut and elsewhere.

Here we observed the general beneficial effect of REV-I on improving gut microbiota composition, reported in previous studies[4,10]. It is also worth mentioning that although previous studies suggested that a product of *A. muciniphila*, which belongs to the phylum *Verrucomicrobia*, possesses metabolic beneficial functions[35], REV-I did show effect on increasing the genus of *Akkermansia* in the current study. Decreased relative abundance of *Akkermansia* was also observed by Sung *et al* in conducting their resveratrol study in mice[4]. Further investigations are needed to expand the investigation into the species level. We have then proved the anti-inflammatory feature of the major microbial metabolite of resveratrol, DHR. This metabolite, as well as 4-hydroxyflavone, possesses anti-inflammatory features in our *in vitro* settings. Nevertheless, they are unlikely the entities in HFR-FE that directly regulate SR-B1.

Among hundreds of compounds identified via metabolomics profiling, we have picked CDCA for a further study, partially due to its heat stable feature. More importantly, recent investigations have revealed that crosstalk between bile acids and microbiome greatly impacts host metabolism[9,27,37,38]. Furthermore, bile acids are among critical components of the gastrointestinal tract that link gut microbiome to metabolism as well as intestinal permeability and inflammation[39]. CDCA, as a major primary bile acid, can be converted into secondary bile acid by microbial modification. As the most potent natural agonist of FXR, CDCA level is known to be elevated after dietary challenge. Hepatic and gastrointestinal FXR, as the principal sensor of bile acids, play a fundamental role in the feedback regulation of bile acid synthesis. Briefly, excessive bile acids contribute to hepatic FXR activation and the expression of SHP, which inhibits transactivation of genes that encode CYP7A1 and CYP8B1, two key enzymes for bile acid synthesis[40]. In the gut, FGF15/FGF19 can be induced by FXR, which may also result in transcriptional repression of CYP7A1[41]. Further investigations on the bile acid/FXR and related signaling cascades may lead to the discovery of multiple novel therapeutic targets for various metabolic disorders[38]. Here we brought this important signaling cascade into the understanding of metabolic beneficial effect of REV-I. As shown in Fig. 7F, in HFD-challenged mice, gut CDCA level rises in response to elevated oral TG intake and local inflammation. In addition to the activation of FXR for triggering the negative feedback loop on bile acid synthesis, CDCA can also activate the NF-κB/SR-B1 signaling cascade, leading to elevated chylomicron secretion. In HFD-challenged mice with REV-I, fecal CDCA level reduction is likely among many events induced by interactions of REV-I and gut microbiota, while this event is at least partially responsible for the attenuation of gut NF-κB/SR-B1 signaling, reduction of chylomicron secretion, and improvement of lipid homeostasis.

Our investigation opens an avenue for mechanistic exploration of how dietary polyphenols exert their metabolic beneficial effects via interacting with gut microbiota, including the regulation of gut bile acid/FXR signaling cascade. One future direction is to dissect exactly how gut microbiome is involved in fecal bile acid homeostasis, including the synthesis, modification, circulation, and fecal elimination of CDCA and other bile acids. Another one is to determine whether the identified CDCA/NF-κB/SR-B1 signaling cascade applies to functions of other dietary polyphenols and other nutraceuticals. Whether the FE from HFD-challenged mice with REV-I possesses entities that can directly repress gut NF-κB/SR-B1 signaling also deserves further investigations.

Declarations

Acknowledgements

This study is supported by Canadian Institutes of Health Research (PJT159735 to TJ and Foundation Grant #353989 to KA), the National Natural Science Foundation of China (grant number 81730090 and 81973022 to WL), and National Institutes of Health operating grant (HL131597 to PWS). JP is a visiting Ph.D. student supported by China Scholarship Council. FR is supported by Canadian Institutes of Health Research doctoral award. We thank Drs. Gary Lewis and Herbert Gaisano (University of Toronto) for data discussion, manuscript editing and suggestions. The authors also thank Metware Biotechnology Co., Ltd (Wuhan, China) for helping with metabolomics profiling and data analyses.

Author Contributions

Conceptualization, Methodology, J.P. and F.R. Formal analysis, J.P. Writing-Original Draft, J.P. Validation, F.R. and W.S. Software and Visualization, A.A.H. Investigation, J.P., F.R., A.A.H, W.S., D.L., G.J. and J.N.F. Resources, C.M. and P.W.S. Supervision and Funding acquisition. X.Q., B.C., K.A., W.L., and T.J. Data Curation, Project administration, and Writing-Review & Editing, K.A., W.L., and T.J.

Declaration of Interests

The authors declare no competing interests.

Methods

Mouse model

We conducted six groups of mouse experiments in total. Experiment 1 generated data for Figure 1, Figure 2 (Panel D-H), Figure 5 and Figure 7 (Panel E). Six-week-old male C57BL/6J mice were fed with low-fat diet (LFD) or high-fat diet (HFD), or HFD with resveratrol (0.5% in diet, designated as HFR) for 8 weeks. The mouse caecum content was collected for 16S rRNA profiling. Experiment 2 generated data for Figure 2 (Panel B-C). Six-week-old male C57BL/6J mice were fed with LFD, or HFD, or HFR (500 mg resveratrol per kg body weight daily by oral gavage) for 12 weeks. Experiment 3 generated data for Figure 3. Six-week-old male intestine mucosa-specific *Scarb1*$^{-/-}$ (*iScarb1*$^{-/-}$) mice or control *Scarb1*$^{fl/fl}$ littermates were fed with HFD without or with resveratrol intervention for 8 weeks. Experiment 4 generated data for Figure 4. Six-week-old male C57BL/6J mice were fed with LFD, HFD or HFR for the first four weeks. Then mice in the HFD and HFR groups were divided into two subgroups and subject to daily oral gavage of BLT-1 (Millipore, Cat#373210), a specific SR-B1 inhibitor, at 3 mg/kg bw or solvent (PBS containing 0.5% DMSO) for two more weeks. Experiment 5 generated data for Figure 6. Six-week-old male C57BL/6J mice were fed with LFD or HFD for the first four weeks. Then Fecal microbiota transplantation (FMT) was conducted as detailed below, followed by metabolic tolerance tests at indicated time. Experiment 6 generated data for Figure 7 (Panel A-C). Six-week-old male C57BL/6J mice were fed with LFD, or HFD, or

HFR (0.5% resveratrol in diet) for 8 weeks. Then fresh feces were collected and extracted for 16S rRNA sequencing and metabolomics analysis.

For experiment 1, 4 and 5, male C57BL/6J mice were purchased from Jackson Laboratory. For experiment 3, *iScarb1*$^{-/-}$ mice were generated by mating floxed SR-B1 (*Scarb1*$^{fl/fl}$) mice[34] with Villin-Cre mice (Jackson Laboratory, Stock#021504). The method for creating *Scarb1*$^{fl/fl}$ mice has been described previously[34]. The primers utilized for genotyping were listed in Supplemental Table 2. Male *iScarb1*$^{-/-}$ mice and control *Scarb1*$^{fl/fl}$ littermates were randomly assigned to experimental groups. Mice were housed under a constant temperature (22°C) and a 12-hour light/dark cycle with *ad libitum* access to food and water (< or = 5 mice per cage). These animal protocols were approved by the University Health Network Animal Care Committee or The Hospital for Sick Children Animal Care Committee and performed in accordance with the guidelines of the Canadian Council of Animal Care. For experiment 2 and 6, male C57BL/6J mice were purchased from Charles River Laboratories. The animal protocols were approved by the Animal Ethics Committee of Sun Yat-sen University. Only male C57BL/6J mice were used in these six experiments because they are more susceptible to diet-induced obesity and metabolic disorders, such as insulin resistance and hypertriglyceridemia.

Cell culture

Human Caco-2 cells (ATCC, Cat#HTB-37, isolated from colon tissue of a 72-year-old white male person) were cultured in Dulbecco's modified Eagle's medium (containing 4.5 g/L glucose) supplemented with 20% fetal bovine serum, 100 units/mL penicillin and 100 μg/mL streptomycin. Cells were grown at 37°C in a 5% CO_2 humid atmosphere. To establish intestinal barrier model, as reported by Briand and colleagues[42], Caco-2 cells were grown for 21 days on microporous PET transwell inserts (23.1 mm, 1 μm pore size, Becton Dickinson Labware) (Figure S4D) until fully differentiated into a monolayer. After a 12-hour starvation (serum-free) period, the monolayers were treated with lipid micelle (containing 1.6 mM oleic acid, 1 mM taurocholic acid sodium, 0.2 mM 1-monooleoylglycerol, 0.05 mM cholesterol, 0.2 mM L-α lysophosphatidylcholine and 0.02 mM BODIPY labelled C_{12} fatty acid), without or with 25 μM resveratrol, or diluted sterile fecal extract (FE) from HFD or HFR-fed mice. For studying chylomicron secretion, media in the lower compartment was collected to measure the concentration of BODIPY labelled C_{12} fatty acid and read at excitation wavelength of 475 nm and emission wavelength of 520 nm with a fluorescence spectrophotometer (Cytation 5, BioTek, USA).

Metabolic tolerance test

Methods for oral glucose tolerance test (OGTT), intraperitoneal insulin tolerance test (IPITT), and fat tolerance test (FTT) have been described previously[24,43]. For OGTT and IPITT, mice were fasted in the morning for 5 hours. Blood glucose levels were determined at 0, 15, 30, 60, 90 and 120 min after oral gavage of glucose at 2 g/kg body weight or intraperitoneal injection of insulin at 0.5 U/kg body weight. To study intestinal chylomicron secretion, we performed fat tolerance test in which mice were fasted overnight prior to oral gavage of olive oil (Sigma-Aldrich, Cat#75348) at 10 ml/kg body weight, and

intraperitoneal injection of poloxamer 407 (Sigma-Aldrich, Cat#P2443) at 1 g/kg body weight to block lipolysis. Blood was then collected from the tail vein at 0, 1, 2 and 4 hours for triglycerides (TG) detection. Triglyceride-rich lipoprotein (TRL) fraction (mainly chylomicron in this context) was isolated as detailed below from mouse plasma collected at the 4^{th} hour of FTT. TRL-TG concentrations were detected by a commercial assay kit (Sigma-Aldrich, Cat#TR0100) and TRL-ApoB48 protein levels were measured by western blotting. To determine TG produced by the liver, mice fasted overnight were injected intraperitoneally with poloxamer 407 at 1 g/kg body weight, and blood was collected from the tail vein at 0, 1, 2 and 4 hours to measure TG levels. Then TRL was isolated and TRL-TG and TRL-ApoB48 levels were measured as stated above.

TRL fraction isolation

Mouse plasma was obtained by centrifuging blood at 8000 rpm for 15 min at 4℃. 150 μL of plasma was used to isolate TRL as we described previously[44]. In brief, 150 μL of plasma was added to the bottom of a centrifugation tube (Beckman Coulter, Cat#344057) containing 4 mL of potassium bromide solution with density of 1.006 g/cm^3. Then the sample was centrifuged in an ultracentrifuge (Beckman Coulter, Optima XE-100) at 35000 rpm for 70 min at 10℃ using a SW55Ti rotor (Beckman Coulter). The top layer of 300 μL was collected as the TRL fraction which was used for measuring TG concentration and ApoB48 level.

Post-heparin plasma LPL activity measurement

LPL is located at the luminal side of capillaries and arteries where it hydrolyzes TG in chylomicron or VLDL to produce free fatty acids. By injection of heparin into the vein, the anchor between LPL and epithelial cells was cleaved and LPL was thus released to circulation in which we can measure its activity by adding an exogenous substrate. In our study, fasted mice were injected through the tail vein with heparin sodium (BioShop, Cat#HPA333.25) at 300 U/kg body weight. Blood was collected 10 min later and centrifuged at 8000 rpm for 15 min at 4℃ to obtain mouse plasma [45]. Then the plasma was used for measuring LPL activity with a commercial fluorescence assay kit (Abcam, Cat#ab204721).

TG intake and fecal TG output measurements

In animal experiment 2, after 11 weeks of HFD feeding, mice were housed individually in metabolic cages. Food intake was recorded daily and TG intake was calculated based on fat content of the diet. Fecal samples were collected daily for three consecutive days. Then feces were lyophilized, ground, and stored at -80℃ before analysis. Fecal TG was measured by an enzymatic assay with a commercial kit (Applygen, Cat#E1013).

Fecal microbiome transplantation (FMT)

Fresh feces were collected from wild-type C57BL/6J mice (donor mice) fed with HFD or HFR for 8 weeks. Feces were collected, homogenized in PBS with 0.05% cysteine HCl and then filtered through a 100 μm

strainer as described by Sung and colleagues[4]. Six-week-old male C57BL/6J mice (recipients) on LFD or HFD for four weeks were administered with PEG3350 at 17 mmol/L in water and fasted overnight to eliminate their gut microbiome before the first FMT. Each mouse then received designated FMT (200 µL, about 40 mg of freshly collected feces) as indicated in Figure 5A for a total of three times on day 1, 3 and 5. Both LFD and HFD-fed recipients received one of the three FMT. Mice received fecal slurry from HFD-fed mice were designated as HFD-FMT group, mice received HFD and resveratrol-fed mice were designated as HFR-FMT group. Another sub-group designated as HFD-FMT+R were included, in which mice received HFD-FMT along with oral gavage of resveratrol at 500 mg/kg body weight on day 1, 3 and 5.

Histological analysis

Oil-red O staining of liver samples was conducted as in our previous study[46]. Fresh mouse liver was embedded in OCT compound (Sakura, Cat#4583) and cut into 8-µm sections. After being fixed in 4% paraformaldehyde for 30 min, the sections were subject to Oil-Red O staining (Sigma-Aldrich, Cat#O0625) dissolved in 60% isopropanol for another 30 min. Then the sections were differentiated in 60% isopropanol and counterstained with Harris hematoxylin. Jejunum samples were fixed in 4% paraformaldehyde for 24 hours and then paraffin-embedded, dewaxed in xylene, rinsed in alcohol, rehydrated, and unmasked in citrate buffer (PH 6.0). After block with protein block solution (Dako, Cat#X0909), sections were incubated with SR-B1 antibody (Abcam, Cat#ab217318, 1:500) for 45 min at 25℃, followed by incubation in Alexa Fluor 555 conjugated anti-rabbit IgG (ThermoFisher Scientific, Cat#A-21428, 1:200) for 30 min at 25℃. Then cell nuclei were counterstained with DAPI, and anti-fade mounting media was applied before immunofluorescence analysis. Alternatively, sections were incubated in ImmPress anti-rabbit IgG (Novus Biologicals, Cat#MP-7401-NB) for 30 min at 25℃ after incubation in SR-B1 primary antibody, developed with DAB substrate and counterstained with Harris hematoxylin for immunohistochemical analysis.

Sterile FE preparation

Two freshly collected fecal pellets (about 40 mg) from mice fed with HFD or HFR for 8 weeks were collected and homogenized in 500 µL PBS. Following a sonication procedure on ice for 1 min twice, and a filtration procedure (through a 0.22 µm strainer), sterile fecal FE was obtained. Then half of the FE from HFR group was heated at 95℃ for 5 min and denoted as the HRH group. The absence of alive bacteria in sterile FE was verified by applying 10 µL FE on Luria broth (LB) agar plate. Thereafter, these sterile FE was diluted and applied to treat Caco-2 cells or intestinal barrier models or subject to metabolomic profiling.

Microbiome profiling and data analyses

DNA was extracted from mouse caecum content or feces using the Qiagen PowerSoil Pro Kit. In brief, the V4 hypervariable region of the 16rRNA gene was amplified using barcoded 515F and 806R primers. Paired end (150bp) sequencing was performed on an Illumina MiSeq platform[47]. The UNOISE pipeline as implemented through USEARCH was used to process raw sequence reads[48]. Cutadapt v.2.6 was used to

trim the last base from all reads. Reads were quality filtered and paired ends reads were assembled to a minimum or maximum length of 243 and 263 (±10 from the mean) base pairs. Next singletons and chimeras were removed. A 99% identity was used to identify operational taxonomic units (OTUs). SINTAX was used to assign taxonomy using USEARCH and the Ribosomal Database Project database v18 available through UNOISE[49]. QIIME1 was used to align OTUs.

OTU tables were rarified to an even depth (12403 reads). Samples were proportionally normalized by dividing read counts by the total number of reads prior to beta-diversity analyses. Bray-Curtis dissimilarity was used to assess community (beta-diversity) differences between groups. Permutational multivariate analyses of variance (PERMANOVAs) were conducted to assess Bray-Curtis beta-diversity differences. Principal coordinate analysis (PCoA) plot was used to visualize beta-diversity differences. The phylum level differences of Bacteroidetes and Firmicutes were assessed using Student-t test and Mann-Whitney nonparametric test and visualized using PRISM. Genus level differences were assessed using Wald test as implemented in DESeq2 and visualized using ggplot2. *p*-values were adjusted for multiple tests using Benjamini-Hochberg correction.

Metabolomics profiling and data analyses

Sterile FE was prepared and stored at -80°C as stated above. Samples were thawed on ice, sonicated for 10 min and centrifuged twice at 12000 rpm for 10 min to discard insoluble particles. The supernatant was collected for LC-ESI-MS/MS analysis. The untargeted metabolomics analysis was performed using a UPLC (ExionLC AD system, AB SCIEX) coupled with a Quadrupole-Time of Flight mass spectrometer (TripleTOF 6600, AB SCIEX). The widely targeted metabolomics profiling was performed using a UPLC coupled to a high-resolution tandem mass spectrometer (QTRAP®, AB SCIEX) controlled by Analyst 1.6.3 software (SCIEX). Samples were separated over an ACQUITY HSS T3 (2.1×100 mm, 1.8 µm) column at 40°C. All samples were equivalently mixed to make quality control (QC) samples and analysed with other samples. A volume of 5 µL of FE was injected into the UPLC-MS. Mobile phases consisted of (A) LC-MS grade water with 0.1% formic acid and (B) acetonitrile with 0.1% formic acid with a flow rate set to 0.4 mL/min. The following gradient was applied: A/B (95/5%) at 0 min, then B to 90% from 0 to 10 min, then B held at 90% from 10 to 11 min, and finally changed to A/B (95/5%) at 11.1 min and held to 14 min. The MS was operated in both positive and negative modes.

ECDF (Empirical Cumulative Distribution Function) was applied to analyze the frequency of QC samples with CV (coefficient of variation) value less than 0.3. More than 90% of QC samples have a CV value < 0.3, indicating a reliable dataset. All raw data was normalized using Quantile normalization and then Log2 transformation was performed before analyses. For principal component analysis (PCA), unit variance scaled data was analyzed by statistics function prcomp within R. Differential metabolites were determined by false discovery rate (FDR) < 0.05 and absolute Log2FC (fold change) ≥ 1. To study the relative abundance of metabolites in different groups, differential metabolites were scaled using unit variance scaling method and then clustered by K-Means method into different subclasses. For pathway enrichment analysis, the KEGG (Kyoto Encyclopedia of Genes and Genomes) database

(http://www.genome.Jp/kegg/) was used to find enriched metabolic signaling pathways involving differential metabolites between two groups. In joint analysis of microbiome and metabolomics data, the relative abundance of the microbiome genus and fecal CDCA and DCA levels were Log10 transformed and then spearman correlation analysis was conducted to compute *r*-value and *p*-value.

Chromatin Immunoprecipitation (ChIP)

NF-κB-p65 binding motifs in human *SCARB1* or rat and mouse *Scarb1* promoters were analyzed through PROMO (version 8.3, http://alggen.lsi.upc.es/). About 60 mg of frozen mouse jejunum samples were ground in liquid nitrogen and kept on dry ice all the time. Samples were cross-linked in PBS containing 1.5% formaldehyde with tubes rotating at room temperature for 15 min and 0.125M glycine solution was added to stop the cross-linking reaction. Then samples were centrifuged and washed with ice-cold PBS twice before homogenizing in PBS until unicellular suspension was obtained. The cells were centrifuged and resuspended in lysis buffer (750 μL per 1×10^7 cells) supplemented with 10 μL/mL PMSF, 1 μL/mL aprotinin and 1 μL/mL leupeptin. Following a sonication procedure to shear DNA to an average fragment size of 200-1000 bp, the lysate was centrifuged and supernatant was transferred to a new tube. 10 μL of chromatin was removed as input. 2 μg of NF-κB-p65 antibody (Cell Signaling Technology, Cat#8242, 1:100) or Rpb (RNA polymerase II) antibody (Cell Signaling Technology, Cat#2629, 1:50) was added into approximately 25 μg of DNA for one immunoprecipitation and the complex was incubated with rocking overnight. 10 μL of blocked staph A was added and incubated for 15 min at room temperature before 150 μL of elution buffer was added to release the chromatin-protein complex. Finally, chromatin was reversed and purified for PCR or real-time PCR using primers listed in Supplemental Table 3.

Reverse transcription and Real-time PCR

Total RNA was extracted from mouse jejunum and Caco-2 cells with Trizol reagent (Invitrogen). Reverse transcription was conducted with a commercial kit (Applied Biosystems, Cat#4368814) and real-time PCR was performed on a real-time PCR system (Applied Biosystems, 7500) using a one-step SYBR Green master mix (Bioline, Cat#BIO-73001) according to manufacturer's protocols. The primers used for amplification of each gene are shown in Supplemental Table 1. At last, the relative expression level of each gene was calculated using the $2^{-\Delta\Delta Ct}$ method normalized by the expression of *Actb* or *ACTB* (which encodes mouse or human β-actin, respectively).

Protein extraction and western blotting

Total cell lysates were obtained by homogenizing mouse jejunum, liver or Caco-2 cell samples in lysis buffer supplemented with protease inhibitors, then 30 μg of boiled lysates were separated by 5-8% SDS-PAGE and blotted onto a nitrocellulose filter membrane (0.45μm, Bio-Rad). After blocking with 7% milk, blots were incubated with anti-SR-B1 (Abcam, Cat#ab217318, 1:3000), anti-ApoB (Midland Bioproducts, Cat#MBC-APB-G1, 1:1000), anti-alpha-Albumin (Nittobo America, Cat#MBC-ALB-G1, 1:1000), anti-NF-κB-p65 (Cell Signaling Technology, Cat#8242, 1:1000), anti-GAPDH (Cell Signaling Technology, Cat#2118, 1:1000), anti-β-actin (Cell Signaling Technology, Cat#3700, 1:1000), anti-alpha-tubulin (Cell Signaling

Technology, Cat#2144, 1:1000) and other antibodies listed in key resources table, followed by corresponding HRP-linked secondary antibodies (Cell Signaling Technology) listed in key resources table. The bands were exposed with an enhanced chemiluminescence kit (Thermo Fisher Scientific, Cat#34580) and semi-quantified using Image J software (version 1.8.0, https://imagej.nih.gov/ij/) normalized by GAPDH, β-actin or alpha-tubulin bands. When needed, blots were stripped with Tris-HCl buffer containing 10% sodium dodecyl sulfate and 0.75% β-mercaptoethanol and incubated at 55℃ for 25 min before re-probed with another primary antibody.

Statistical analysis

Results are presented as mean ± standard deviation (SD). Comparisons between groups were performed using an unpaired two-tailed t-test, Mann-Whitney nonparametric test (between two groups), one-way analysis of variance (ANOVA) followed by the Dunnett's *post hoc* test (compared to HFD or PBS group), or two-way ANOVA (for mice of different genetic background and diet) followed by Sidak's *post hoc* test where appropriate. All of the statistical details of experiments can be found in the figure legends in which the n number means biological replicates in all experiments. Statistical analyses were performed with GraphPad Prism 8.0 (GraphPad Software, La Jolla, CA, USA). *, $^{\#}$, or $^{\&}$, P<0.05; **, $^{\#\#}$, or $^{\&\&}$, P<0.01; ***, $^{\#\#\#}$, or $^{\&\&\&}$, P<0.001.

References

1. Li, Y., *et al.* Hepatic SIRT1 attenuates hepatic steatosis and controls energy balance in mice by inducing fibroblast growth factor 21. Gastroenterology **146**, 539–549 e537 (2014).
2. Anhe, F.F., *et al.* A polyphenol-rich cranberry extract protects from diet-induced obesity, insulin resistance and intestinal inflammation in association with increased Akkermansia spp. population in the gut microbiota of mice. Gut **64**, 872–883 (2015).
3. Cote, C.D., *et al.* Resveratrol activates duodenal Sirt1 to reverse insulin resistance in rats through a neuronal network. Nat Med **21**, 498–505 (2015).
4. Sung, M.M., *et al.* Improved Glucose Homeostasis in Obese Mice Treated With Resveratrol Is Associated With Alterations in the Gut Microbiome. Diabetes **66**, 418–425 (2017).
5. Zang, M., *et al.* Polyphenols stimulate AMP-activated protein kinase, lower lipids, and inhibit accelerated atherosclerosis in diabetic LDL receptor-deficient mice. Diabetes **55**, 2180–2191 (2006).
6. Breton, J., *et al.* Gut Commensal E. coli Proteins Activate Host Satiety Pathways following Nutrient-Induced Bacterial Growth. Cell Metab **23**, 324–334 (2016).
7. Tian, L. & Jin, T. The incretin hormone GLP-1 and mechanisms underlying its secretion. J Diabetes **8**, 753–765 (2016).
8. Wang, D., *et al.* Gut microbiota metabolism of anthocyanin promotes reverse cholesterol transport in mice via repressing miRNA-10b. Circ Res **111**, 967–981 (2012).

9. Wu, Q., *et al.* Intestinal hypoxia-inducible factor 2alpha regulates lactate levels to shape the gut microbiome and alter thermogenesis. Cell Metab **33**, 1988–2003 e1987 (2021).
10. Bird, J.K., Raederstorff, D., Weber, P. & Steinert, R.E. Cardiovascular and Antiobesity Effects of Resveratrol Mediated through the Gut Microbiota. Adv Nutr **8**, 839–849 (2017).
11. Wang, P., *et al.* Resveratrol reduces obesity in high-fat diet-fed mice via modulating the composition and metabolic function of the gut microbiota. Free Radic Biol Med **156**, 83–98 (2020).
12. Hogue, J.-C., *et al.* Evidence of increased secretion of apolipoprotein B-48-containing lipoproteins in subjects with type 2 diabetes. Journal of Lipid Research **48**, 1336–1342 (2007).
13. Duez, H.l.n., *et al.* Hyperinsulinemia Is Associated With Increased Production Rate of Intestinal Apolipoprotein B-48 Containing Lipoproteins in Humans. Arteriosclerosis, Thrombosis, and Vascular Biology **26**, 1357–1363 (2006).
14. Nordestgaard, B.G., Benn, M., Schnohr, P. & Tybjærg-Hansen, A. Nonfasting Triglycerides and Risk of Myocardial Infarction, Ischemic Heart Disease, and Death in Men and Women. JAMA **298**, 299–308 (2007).
15. Nordestgaard, B.G. & Varbo, A. Triglycerides and cardiovascular disease. Lancet **384**, 626–635 (2014).
16. Ginsberg, H.N., *et al.* Triglyceride-rich lipoproteins and their remnants: metabolic insights, role in atherosclerotic cardiovascular disease, and emerging therapeutic strategies-a consensus statement from the European Atherosclerosis Society. Eur Heart J **42**, 4791–4806 (2021).
17. Donnelly, K.L., *et al.* Sources of fatty acids stored in liver and secreted via lipoproteins in patients with nonalcoholic fatty liver disease. J Clin Invest **115**, 1343–1351 (2005).
18. Hussain, M.M., *et al.* Clearance of chylomicron remnants by the low density lipoprotein receptor-related protein/alpha 2-macroglobulin receptor. J Biol Chem **266**, 13936–13940 (1991).
19. Ko, C.W., Qu, J., Black, D.D. & Tso, P. Regulation of intestinal lipid metabolism: current concepts and relevance to disease. Nat Rev Gastroenterol Hepatol **17**, 169–183 (2020).
20. Xiao, C., Stahel, P., Carreiro, A.L., Buhman, K.K. & Lewis, G.F. Recent Advances in Triacylglycerol Mobilization by the Gut. Trends Endocrinol Metab **29**, 151–163 (2018).
21. Nauli, A.M., *et al.* CD36 is important for chylomicron formation and secretion and may mediate cholesterol uptake in the proximal intestine. Gastroenterology **131**, 1197–1207 (2006).
22. Hayashi, A.A., *et al.* Intestinal SR-BI is upregulated in insulin-resistant states and is associated with overproduction of intestinal apoB48-containing lipoproteins. American Journal of Physiology-Gastrointestinal and Liver Physiology **301**, G326-G337 (2011).
23. Stahl, A., *et al.* Identification of the major intestinal fatty acid transport protein. Mol Cell **4**, 299–308 (1999).
24. Lino, M., *et al.* Intestinal scavenger receptor class B type I as a novel regulator of chylomicron production in healthy and diet-induced obese states. American Journal of Physiology-Gastrointestinal and Liver Physiology **309**, G350-G359 (2015).

25. Hansen, G.H., Niels-Christiansen, L.L., Immerdal, L. & Danielsen, E.M. Scavenger receptor class B type I (SR-BI) in pig enterocytes: trafficking from the brush border to lipid droplets during fat absorption. Gut **52**, 1424–1431 (2003).
26. Miyata, S., Inoue, J., Shimizu, M. & Sato, R. 4'-Hydroxyflavanone suppresses activation of sterol regulatory element-binding proteins and de novo lipid synthesis. FEBS letters **586**, 1778–1782 (2012).
27. Sun, L., *et al.* Gut microbiota and intestinal FXR mediate the clinical benefits of metformin. Nat Med **24**, 1919–1929 (2018).
28. Dash, S., Xiao, C., Morgantini, C., Szeto, L. & Lewis, G.F. High-Dose Resveratrol Treatment for 2 Weeks Inhibits Intestinal and Hepatic Lipoprotein Production in Overweight/Obese Men. Arterioscler Thromb Vasc Biol **33**, 2895–2901 (2013).
29. Jin, T., Song, Z., Weng, J. & Fantus, I.G. Curcumin and other dietary polyphenols: potential mechanisms of metabolic actions and therapy for diabetes and obesity. Am J Physiol Endocrinol Metab **314**, E201-E205 (2018).
30. Krieger, M. Scavenger receptor class B type I is a multiligand HDL receptor that influences diverse physiologic systems. J Clin Invest **108**, 793–797 (2001).
31. Armstrong, S.M., *et al.* A novel assay uncovers an unexpected role for SR-BI in LDL transcytosis. Cardiovasc Res **108**, 268–277 (2015).
32. Saddar, S., *et al.* Scavenger receptor class B type I is a plasma membrane cholesterol sensor. Circ Res **112**, 140–151 (2013).
33. Rosenson, R.S., *et al.* Cholesterol efflux and atheroprotection: advancing the concept of reverse cholesterol transport. Circulation **125**, 1905–1919 (2012).
34. Huang, L., *et al.* SR-B1 drives endothelial cell LDL transcytosis via DOCK4 to promote atherosclerosis. Nature **569**, 565–569 (2019).
35. Plovier, H., *et al.* A purified membrane protein from Akkermansia muciniphila or the pasteurized bacterium improves metabolism in obese and diabetic mice. Nat Med **23**, 107–113 (2017).
36. Anhe, F.F., *et al.* A polyphenol-rich cranberry extract reverses insulin resistance and hepatic steatosis independently of body weight loss. Mol Metab **6**, 1563–1573 (2017).
37. Wu, Q., *et al.* Suppressing the intestinal farnesoid X receptor/sphingomyelin phosphodiesterase 3 axis decreases atherosclerosis. J Clin Invest **131**(2021).
38. Sun, L., Cai, J. & Gonzalez, F.J. The role of farnesoid X receptor in metabolic diseases, and gastrointestinal and liver cancer. Nat Rev Gastroenterol Hepatol **18**, 335–347 (2021).
39. Jia, W., Xie, G. & Jia, W. Bile acid-microbiota crosstalk in gastrointestinal inflammation and carcinogenesis. Nat Rev Gastroenterol Hepatol **15**, 111–128 (2018).
40. Goodwin, B., *et al.* A regulatory cascade of the nuclear receptors FXR, SHP-1, and LRH-1 represses bile acid biosynthesis. Mol Cell **6**, 517–526 (2000).

41. Kong, B., *et al.* Mechanism of tissue-specific farnesoid X receptor in suppressing the expression of genes in bile-acid synthesis in mice. Hepatology (Baltimore, Md.) **56**, 1034–1043 (2012).
42. Briand, O., *et al.* Liver X Receptor Regulates Triglyceride Absorption Through Intestinal Down-regulation of Scavenger Receptor Class B, Type 1. Gastroenterology **150**, 650–658 (2016).
43. Ip, W., *et al.* Liver-specific expression of dominant-negative transcription factor 7-like 2 causes progressive impairment in glucose homeostasis. Diabetes **64**, 1923–1932 (2015).
44. Hsieh, J., *et al.* Glucagon-like peptide-2 increases intestinal lipid absorption and chylomicron production via CD36. Gastroenterology **137**, 997–1005, 1005.e1001-1004 (2009).
45. Yagyu, H., *et al.* Lipoprotein lipase (LpL) on the surface of cardiomyocytes increases lipid uptake and produces a cardiomyopathy. J Clin Invest **111**, 419–426 (2003).
46. Liu, D., *et al.* Hepatic fibroblast growth factor 21 is involved in mediating functions of liraglutide in mice with dietary challenge. Hepatology (Baltimore, Md.) **74**, 2154–2169 (2021).
47. Oliva, M., *et al.* Transitions in oral and gut microbiome of HPV + oropharyngeal squamous cell carcinoma following definitive chemoradiotherapy (ROMA LA-OPSCC study). British journal of cancer **124**, 1543–1551 (2021).
48. Edgar, R.C. UPARSE: highly accurate OTU sequences from microbial amplicon reads. Nature methods **10**, 996–998 (2013).
49. Wang, Q., Garrity, G.M., Tiedje, J.M. & Cole, J.R. Naive Bayesian classifier for rapid assignment of rRNA sequences into the new bacterial taxonomy. Applied and environmental microbiology **73**, 5261–5267 (2007).

Figures

Figure 1

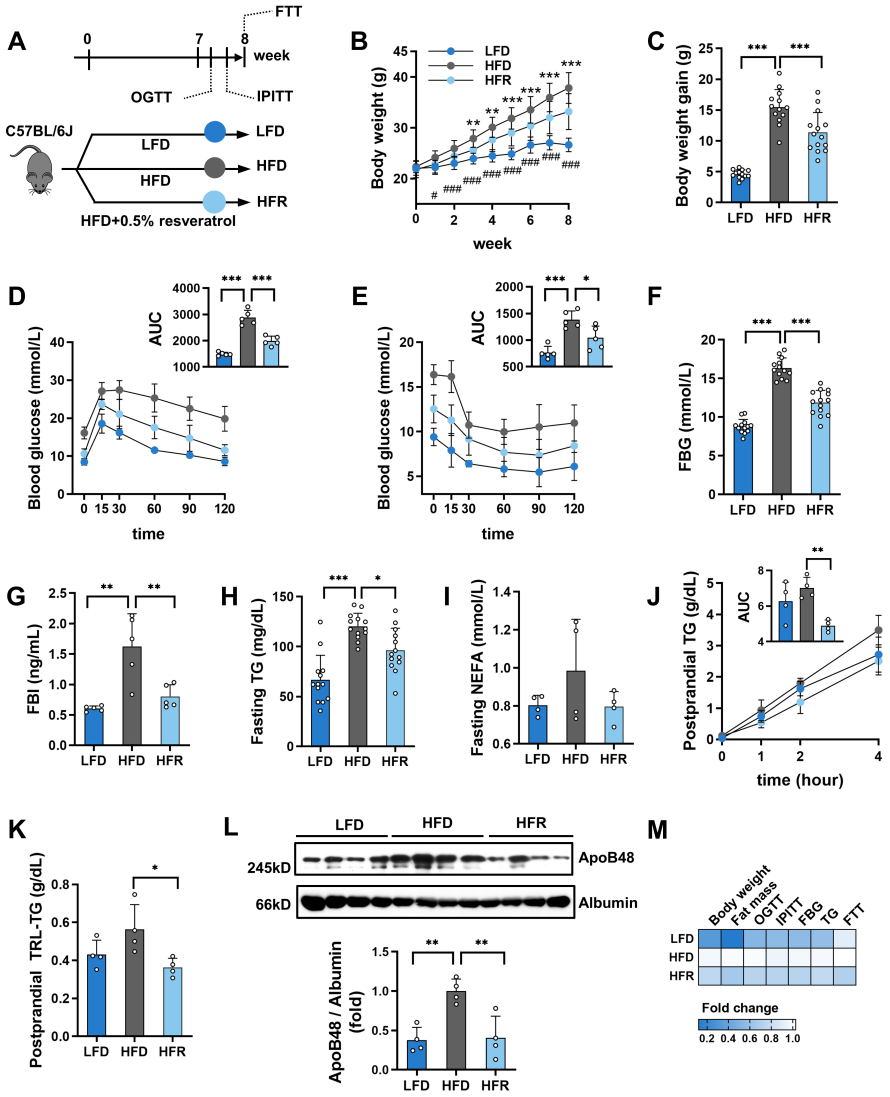

Figure 1

REV-I reduces chylomicron production in HFD-challenged mice. (A) Diagram shows experimental procedures. **(B, C)** Body weight **(B)** and body weight gain (**C)** at the end of the 8th week; n=13-14. **(D, E)** Blood glucose level and area under the curve (AUC) during OGTT **(D)** and IPITT **(E)**; n=5. **(F-I)** Fasting blood glucose (FBG) **(F)** (n=13-14), insulin (FBI) **(G)** (n=5), TG **(H)** (n=13-14) and non-esterified FA (NEFA) levels **(I)** (n=4) at the end of the 8thweek. **(J)** Postprandial TG levels during FTT, n=4. **(K, L)**Postprandial

plasma collected 4 h after olive oil gavage was ultracentrifuged for isolating TRL (mainly chylomicron). TG concentrations were then measured **(K)**, while ApoB48 levels were assessed by Western blotting **(L)**; n=4. **(M)** Heatmap summarizes metabolic effects of REV-I presented in Figure 1 (fold change of a given parameter vs that in HFD-fed mice which is defined as 1-fold). One-way ANOVA with Dunnett's *post hoc* test (compared to HFD group). *or #$P < 0.05$, **$P < 0.01$, ***or ###$P < 0.001$. For panel B, ** or ***, HFR vs HFD; # or ###, LFD vs HFD. See also Figure S1.

Figure 2

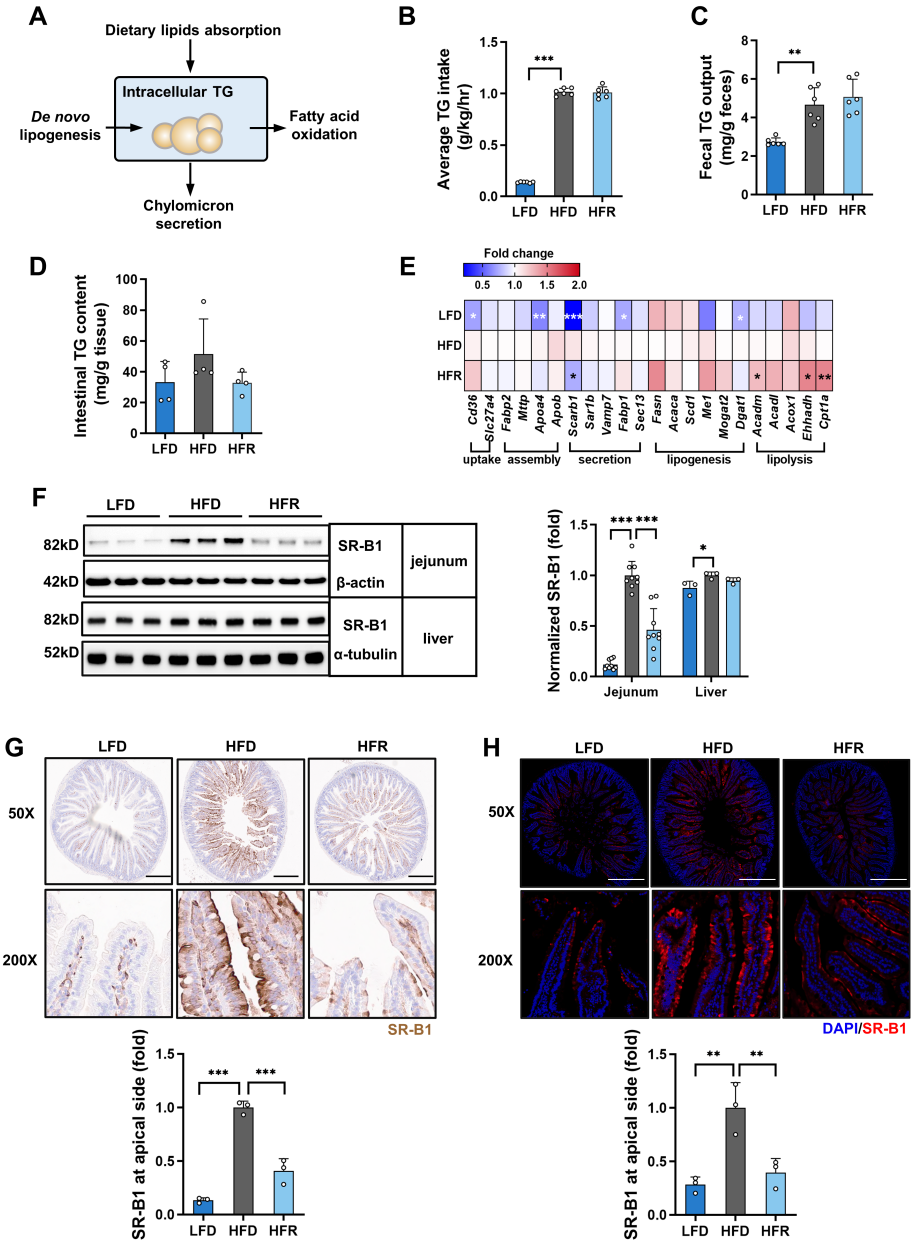

Figure 2

REV-I reduces jejunal but not liver SR-B1. (A) Diagram summarizes metabolic processes involved in intestinal lipid (TG) homeostasis. **(B, C)** Average TG intake **(B)** and daily fecal TG loss **(C)** of mice individually housed in metabolic cages at the end of the 8thweek; n=6. **(D)** Jejunal intracellular TG contents; n=4. **(E)**Heatmap shows the expression of genes involved in intestinal lipid metabolism among the three groups of mice (see statistical analysis results of qRT-PCR in Table S4); n=12. **(F)** Jejunal (n=9) and hepatic (n=3) SR-B1 levels were assessed by Western blotting. **(G)** Representative jejunum SR-B1 immunostaining images (brown), along with its quantitative scores at the apical membrane. The scale bar is 300 μm; n=3. **(H)** Representative jejunum SR-B1 immunofluorescence staining images (red), along with its quantitative scores at the apical membrane. The scale bar is 500 μm; n=3. One-way ANOVA with Dunnett's *post hoc*test (compared to HFD group). **P* < 0.05, ***P* < 0.01, ****P*< 0.001.

Figure 3

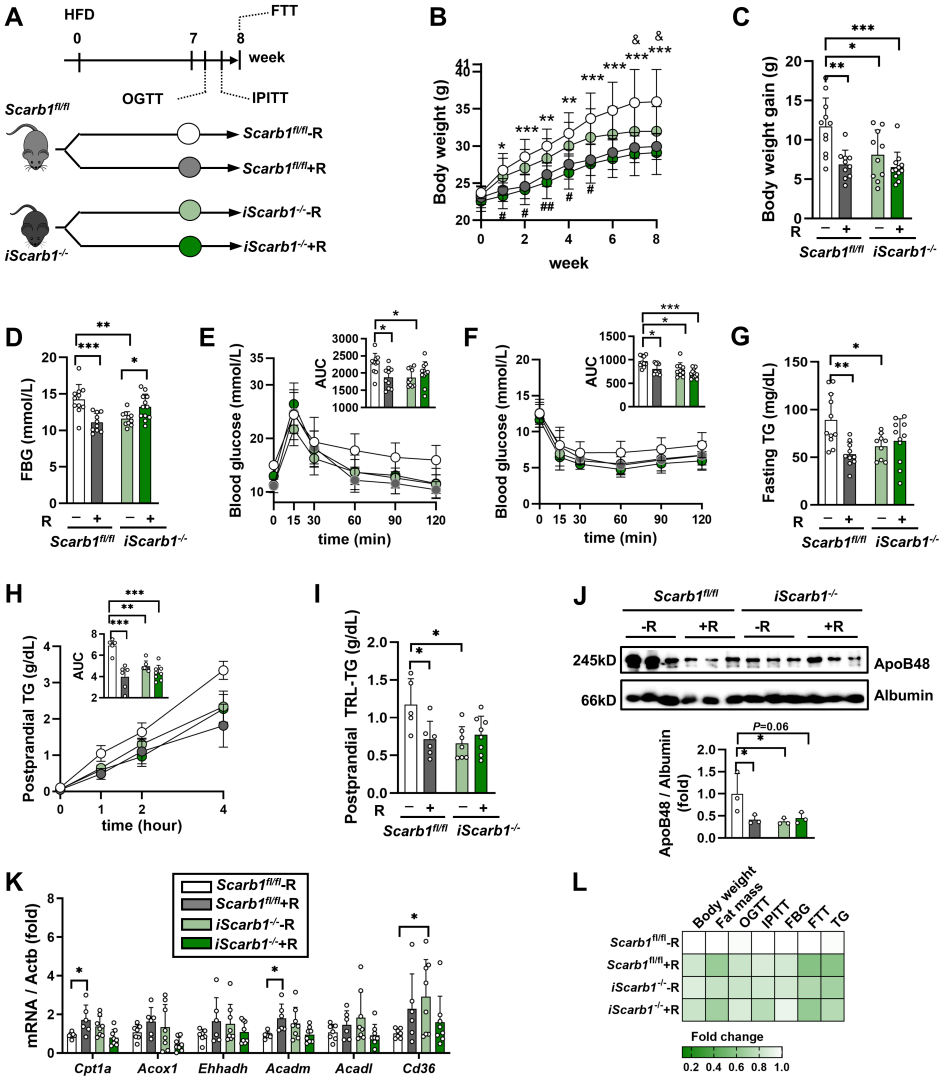

Figure 3

Intestinal mucosa specific SR-B1 KO mice show lack of further response to REV-I. (A) Diagram shows experimental procedures in *Scarb1fl/fl* and *iScarb1-/-*mice. **(B, C)** Body weight **(B)** and body weight gain **(C)** at the end of the 8th week; n=10-12. **(D)** Fasting blood glucose (FBG) levels at the end of the 8th week; n=10-12. **(E, F)**Blood glucose levels and AUC during OGTT **(E)** and IPITT **(F)**, n=10-12. **(G)** Fasting TG levels at the 8th week; n=10-12. **(H)**Postprandial TG levels during FTT; n=5-8. **(I-J)** Postprandial plasma

collected 4 h after olive oil gavage was ultracentrifuged for isolating TRL. TG concentrations were then measured **(I)**, and ApoB48 levels were assessed **(J)** (albumin as loading control); n=3. **(K)** Expression of *Cd36* and other genes that are involved in FA β-oxidation; n=5-8. **(L)**Heatmap summarizes metabolic effects of REV-I presented in Figure 3. A given parameter in *Scarb1fl/fl* control mice without REV-I is defined as 1-fold. Two-way ANOVA with Šidák *post hoc* test. *or #or &$P < 0.05$, **or ##$P < 0.01$, ***$P < 0.001$. For panel B, *, **, or ***, *Scarb1fl/fl*+R vs *Scarb1fl/fl*-R; # or ##, *iScarb1-/-*+R vs *iScarb1-/-*–R; &, *Scarb1fl/fl* -R vs *iScarb1-/-*–R. See also Figure S2.

Figure 4

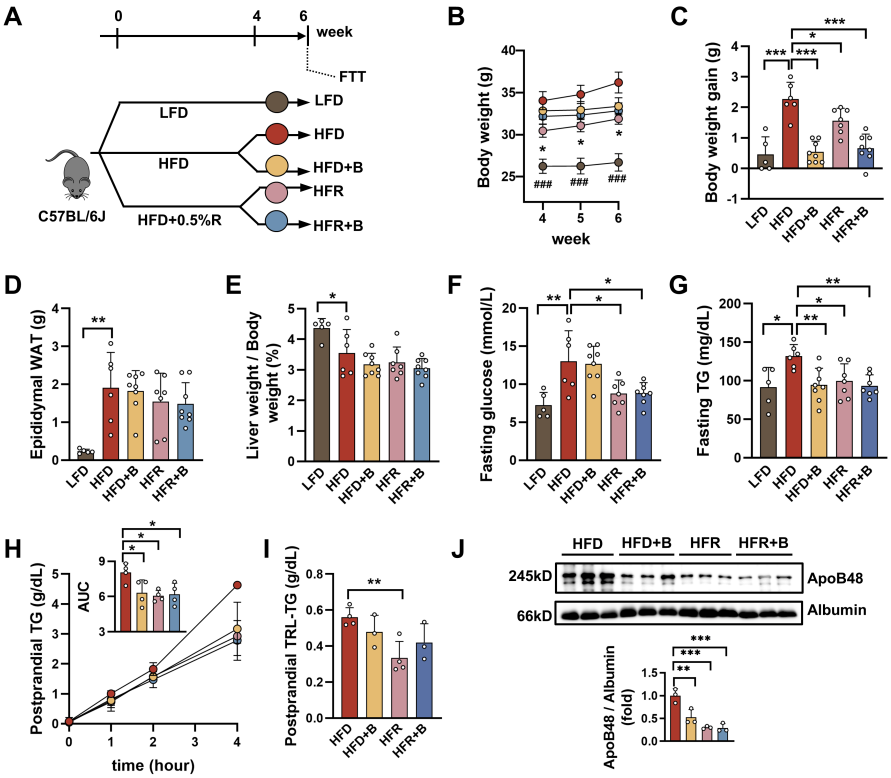

Figure 4

BLT-1 gavage generates no additive effect with REV-I. **(A)** Diagram shows the experimental procedures in C57BL/6J mice treated with resveratrol (HFR), or BLT-1 (B), or both (HFR+B). **(B, C)** Body weight **(B)** and body weight gain **(C)** from week 4-6; n=5-8. **(D-G)** Epididymal white adipose tissue **(D)**, liver weight to body weight ratio **(E)**, fasting glucose **(F)**, and TG levels **(G)** at the end of the 6thweek; n=5-8. **(H)** Plasma TG levels during FTT; n=4. **(I, J)**Postprandial plasma collected 4 h after olive oil gavage was ultracentrifuged for isolating TRL. TG concentrations were then measured **(I)**, and ApoB48 levels were assessed by Western blotting **(J)**; n=3. One-way ANOVA with Dunnett's *post hoc* test (compared to HFD group). **P* < 0.05, ***P*< 0.01, ***or ###*P* < 0.001. For panel B, *, HFD vs HFR; ###, LFD vs HFD.

Figure 5

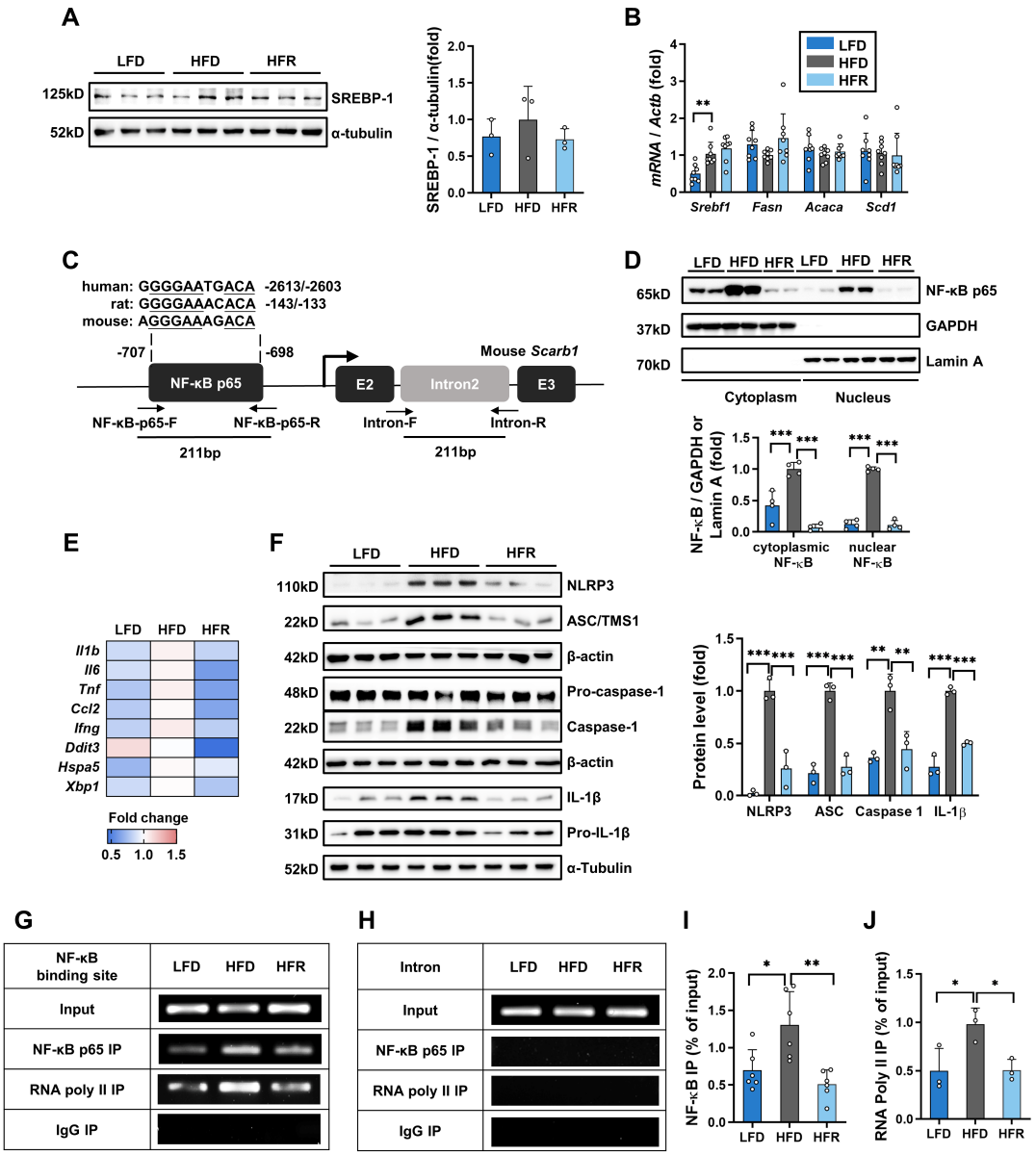

Figure 5

REV-I represses jejunal SR-B1 involving reduced transcriptional activity of NF-κB-p65. (A) Jejunum expression of SREBP-1 detected by Western blotting; n=3. **(B)** Comparison of expression of *Srebf1* (which encodes SREBP-1) and its target genes in jejunum; n=8. **(C)** Location of the conserved NF-κB p65 binding motif within human, rat and mouse *SCARB1*/*Scarb1* promoters and nucleotide primers utilized in ChIP and qChIP. **(D)** Detection of cytoplasmic and nucleus NF-κB-p65 by Western blotting in the jejunum of

indicated groups of mice, presented in Figure 1; n=4. The blot of NF-κB-p65 was stripped to re-probe for Lamin A. **(E)** Heatmap shows the comparison of intestinal inflammatory genes that are known to be regulated by NF-κB in the jejunum; n=8 (see statistical analysis results of qRT-PCR in Table S6). **(F)** Western blotting shows the relative expression of inflammasome components in the jejunum. n=3. The blot of Pro-caspase-1 was stripped and rre-probed for β-actin. **(G, H)** ChIP shows the binding of NF-κB or RNA Polymerase II to the mouse *Scarb1* promoter **(G)**but not the intron region **(H)** in the jejunum. n=3-6. **(I, J)** qChIP shows the comparison of binding of NF-κB **(I)** or RNA Polymerase II **(J)**to mouse *Scarb1* promoter in the jejunum. n=3-6. One-way ANOVA with Dunnett's *post hoc* test (compared to HFD group). $*P < 0.05$, $**P < 0.01$, $***P < 0.001$.

Figure 6

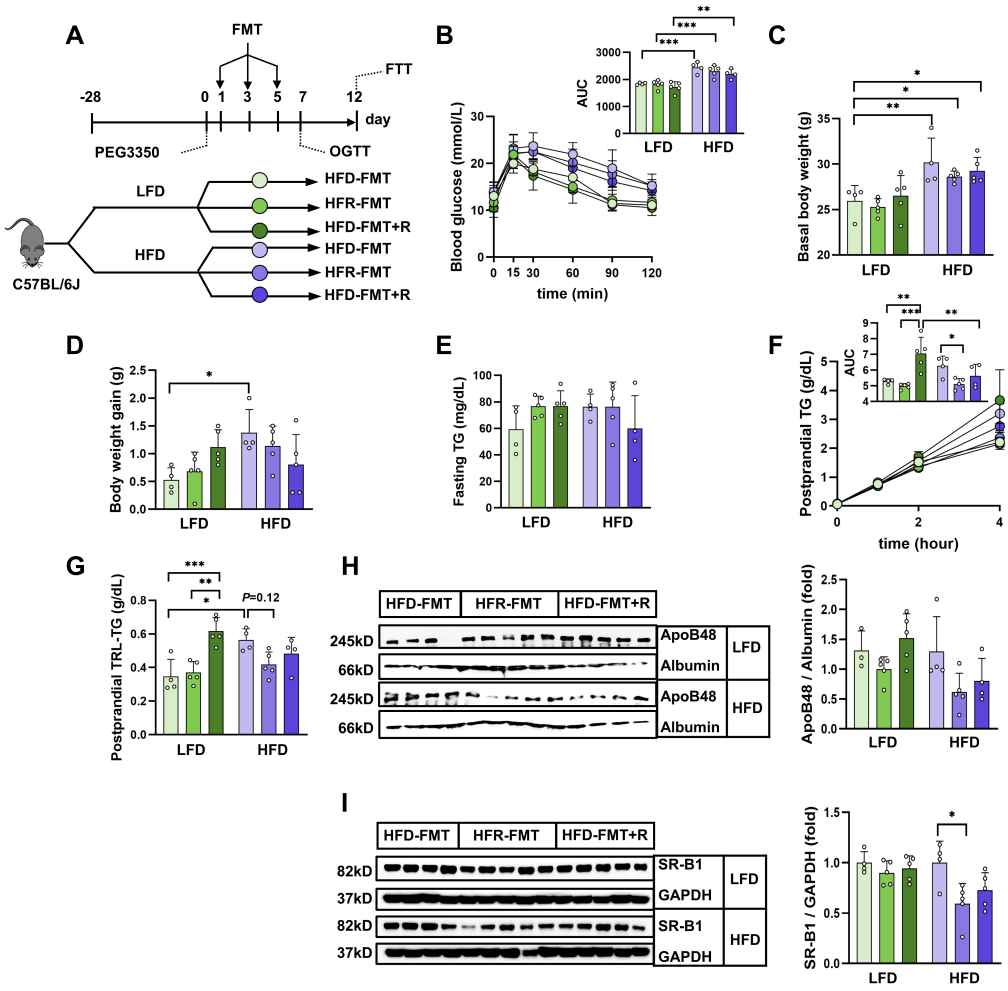

Figure 6

The inhibitory effect of REV-I on SR-B1 involves gut microbiota. (A) Diagram shows the design of the short-term FMT. Six-week-old male mice on LFD or HFD for four weeks were further divided randomly into three groups, receiving indicated FMT following PEG3350 treatment. **(B)** Blood glucose level and AUC during OGTT on day 7. **(C)** Basal body weight before FMT. **(D)** Body weight gain between day 0 and day 12. **(E)** Fasting TG level on day 12. **(F)**Postprandial TG level during FTT at day 12. **(G, H)** Postprandial

plasma collected 4 h after olive oil gavage was ultracentrifuged to isolate TRL. TG concentrations were then measured **(G)**, and ApoB48 levels were assessed by Western blotting **(H)**. **(I)** Jejunal SR-B1 level. n=4-5 for each test. Two-way ANOVA with Šidák *post hoc* test. **P* < 0.05, ***P*< 0.01, ****P* < 0.001. See also Figure S3, S4, and S5.

Figure 7

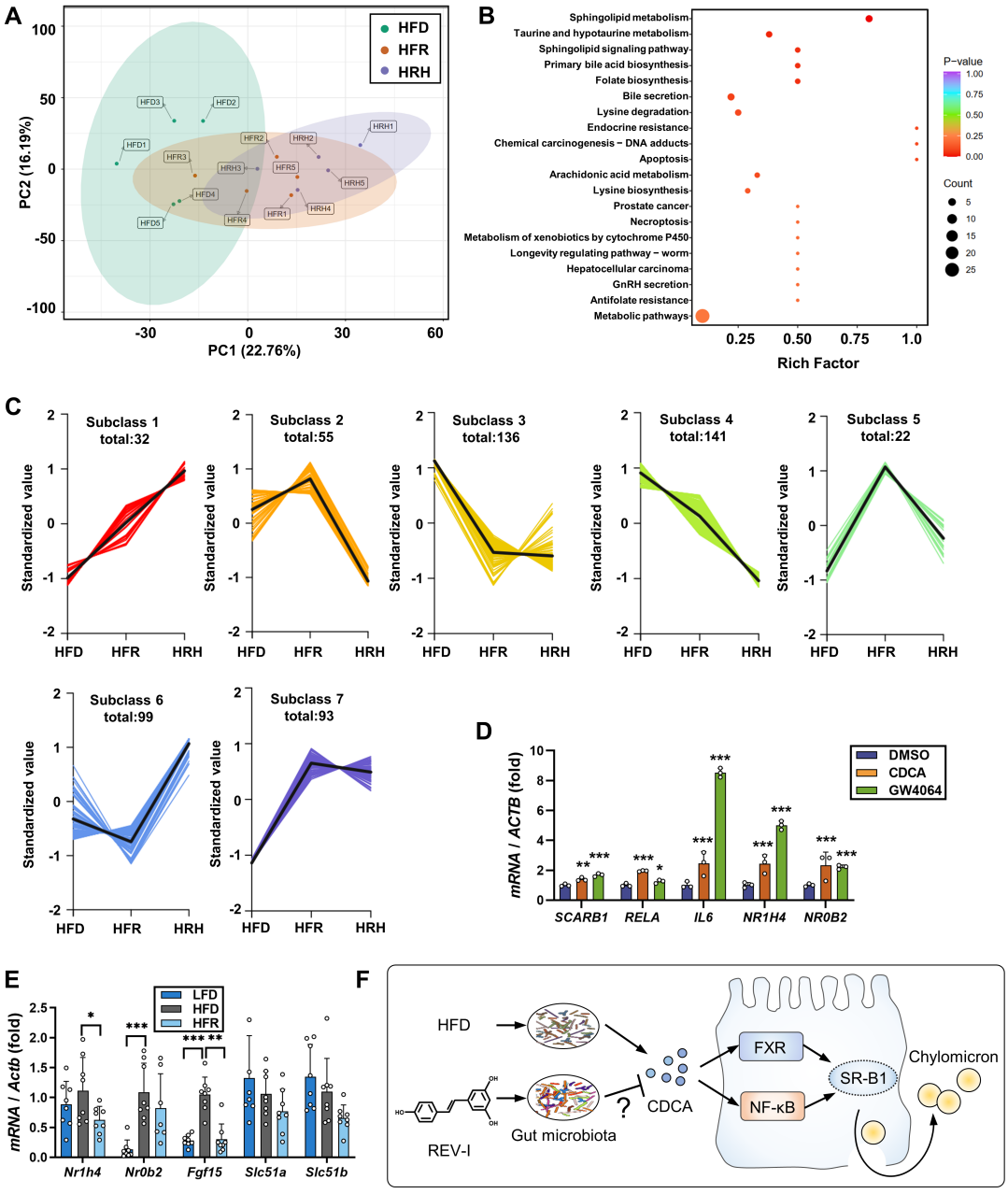

Figure 7

REV-I attenuates HFD induced fecal CDCA elevation while CDCA stimulates NF-κB and SR-B1 in Caco-2 cells. (A) Principal component analysis (PCA) plot. Sterile FEs from the designated group were subjected to untargeted metabolomics analysis. HRH, sterile FE isolated from mice on HFR feeding was heated at 95℃ for 5 min; n=5. **(B)** KEGG pathway enrichment analysis shows the top 20 regulated metabolic pathways by REV-I. Rich Factor was determined by the ratio of differential metabolites detected vs total metabolites in that pathway. **(C)** K-Means cluster analysis divided all the differential metabolites into 7 subclasses according to their relative abundance in different groups. Only subclasses 3 and 7 show comparable levels in HFR and HRH groups. **(D)** Comparison of *SCARB1*, *RELA*, *IL6*, *NR1H4* (which encodes FXR) and *NR0B2* (which encodes SHP) levels in Caco-2 cells treated without or with CDCA (200 μM), or GW4064 (25 μM) for 8 h; n=3. **(E)** Comparison of expression of indicated genes in jejunum of indicated mice (Presented in Figure 1A); n=8. **(F)** The illustration shows that HFD challenge increases levels of CDCA, which is a natural agonist of FXR, while REV-I attenuates HFD-induced fecal CDCA elevation, possibly by altering gut microbiome composition. The attenuation of CDCA production also results in reduced gut FXR and NF-κB transcriptional activity, leading to lower SR-B1 expression and chylomicron secretion. One-way ANOVA with Dunnett's *post hoc* test compared to DMSO group (E) or HFD group (F). **P* < 0.05, ***P* < 0.01, ****P*< 0.001. See also Figure S6-S7.

Supplementary Files

This is a list of supplementary files associated with this preprint. Click to download.

- supplementalinformation0908.docx